Numerical simulation of the multi-component injection moulding process

W. F. Zoetelief, G. W. M. Peters and H. E. H. Meijer*

CPC, Centre for Polymers and Composites, Eindhoven University of Technology, Eindhoven, The Netherlands

Numerical Simulation of the Multi-Component Injection Moulding Process

The versatility of the injection moulding process can be increased by combining multiple polymers in one product. The multi-component injection moulding process (MCIM) offers the possibility to inject two or three materials sequentially or simultaneously into a mould to make products that consist of e.g. a layered structure. For a successful application of this technique for geometrically complex products or multiple materials, the material distribution in the product has to be predicted. In this paper numerical tools are described for calculating the positions of material particles during the flow in the mould cavity. These tools make it possible to solve the inverse problem of predicting the injection sequence in MCIM given a required material distribution in the product. The simulations are validated using experimental results of a co-injected strip with stiffener ribs. Furthermore the effect of a bifurcation of the midsurface on the material distribution is investigated numerically using a simplified model based on the local mass balance.

1 Introduction

In the multi-component injection moulding (MCIM) process, two or three polymer materials are sequentially or simultaneously injected in the mould to make products with e.g. a layered structure. The distribution of the layers in the product depends on the position of the gate, the geometry of the injection nozzle and the injection sequence (simultaneous and/or sequential). By changing this sequence (A,B; A,B,A; A/B; A,A/B,A; etc.) the thickness and place (centric or eccentric) of the resulting layers can be controlled (Fig. 1). This multi-component injection technology differs from the multi-shot technology. In this last technique the first shot is placed after complete solidification into a larger mould-cavity followed by the injection of a second shot against or around the previous shot.

The MCIM technique was originally developed by ICI in 1967 [1]. The process aimed at the production of large, light-weight, and stiff products. The sequential injection of two components (A,B; A,B,A) limited the practical applications to simply shaped sandwich constructions with three layers. The component B, the core layer, typically consisted of the A material with a physical or chemical foaming agent. In this way, large parts with hard, flat, and glossy skin layers could be moulded without the need for high clamping forces since shrinkage was compensated for by the expansion of the core material (instead of by packing at high pressures as in the conventional injection moulding process). In applications where thin-walled products are more suitable, light-weight, high-stiffness products can be moulded more economically using reinforcing ribs.

During the last decade, the MCIM technology has been evaluated also for thin-walled products using the Battenfeld two-channel technique [2]. With this technique not only sequential injection is possible as in the ICI technique, but also simultaneous injection of two components (A,A/B,A; A,B/A,A). In this way, thin, eccentric layers could be realized in a product. Examples of applications are: shielding against electro-magnetic interference (EMI) by a conductive layer inside the product [2, 3], applying a special barrier material in the core [2, 4], recycling of thermoplastic materials with scrap material in the core [5] and a thin (eccentric) laser-writable layer of a special polymer moulded just below the surface.

The sandwich moulding technique has been used in the past also to acquire insight in the mould filling process [6, 7]. For isothermal conditions it was found that the most uniform skin-core structures occurred when the first injected melt possessed a lower viscosity than the second. Moreover, in case of simultaneous injection of two materi-

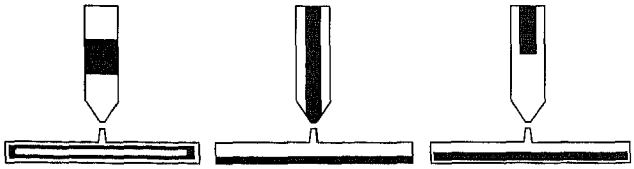

Fig. 1. Idealized representation of two component injection moulding with sequential (A,B,A), simultaneous (A/B), and combined (A,A/B) injection

* Mail address: Wim F. Zoetelief, Philips Research, Prof. Holstlaan 4, 5656 AA Eindhoven, Netherlands

als, the melt with the lower viscosity did encapsulate the melt with the higher viscosity during the flow in the runner section.

Today, the numerical simulation of the injection moulding process is directed towards the prediction of the final properties of injection moulding products rather than solely analysing the mouldability of a product. Despite, upto now not much attention has been paid to the modelling of the MCIM process. Turng et al. [8] described the sequential injection of two (different) polymers by calculating the residence time of particles that enter the mould cavity. They were able to predict the position of the interface between the two materials. Their method is restricted to the sequential injection of two materials with one switch-over time. Schlatter et al. [9] used a special transport equation to track the interface for sequential injection of polymers. Vos et al. [10] and Peters et al. [11] gave examples of both sequential and simultaneous injection using a conservation of identity method for locating the different materials during the process. In this paper, the latter method is employed for the prediction of the material distribution in the MCIM process. Furthermore, an inverse procedure is developed in order to predict the injection configuration once the desired final material distribution in the product is given.

2 Modelling the MCIM Process

The set of equations, needed to describe moulding processes, consists of the balance equations and the constitutive equations, completed with the proper set of boundary and initial conditions. This set of governing equations can be reduced considerably by assuming that mould cavities consist of narrow, weakly curved channels. Therefore, the Hele-Shaw or thin film approximation can be employed [12 to 16]. Since modelling of the MCIM process is almost identical to modelling of conventional injection moulding (see e.g. [12, 13, 15 to 19]), the derivation of the basic equations is not repeated here.

A generalized Newtonian fluid model is used, since neglection of viscoelasticity of the polymers proved to be not too serious [15, 20] mainly because the boundary and initial conditions are given as prescribed velocities and flow rates. Thus the balance of mass and the simple kinematics dominate the transient flow. Here the Cross model is used for which the viscosity is given by

$$\eta(p,T,\dot{\gamma}) = \frac{\eta_0}{1 + (\eta_0\dot{\gamma}/\tau^*)^{1-n}} \qquad (1)$$

where $\eta = \eta_0(p,T)$ is the zero shear rate viscosity, τ^* and n are constants. The double-domain Tait [21] equation is used to model the pvT-behaviour. In the cases considered here only one domain, i.e. the molten state, is of importance. The thermal properties of the polymer are considered constant in the molten as well as in the solid state.

2.1 Particle Tracking

Particles are abstract distinct points in the flow that have to be followed in time and space. Using similar definitions, particle tracking got considerable attention in numerical simulations of non-Newtonian flows employing memory

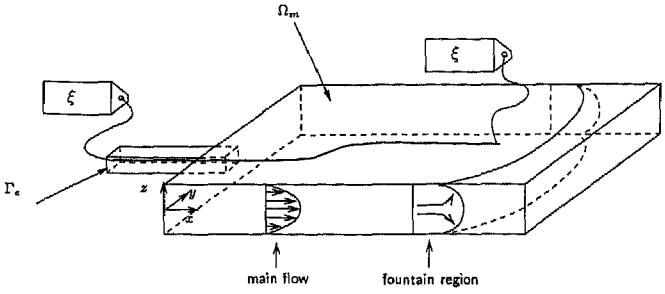

Fig. 2. Flow regions in the Hele-Shaw approximation

integral equations (see e.g. [22 to 24]). The particle paths can be constructed by integrating the reversed velocity field starting from every nodal point in the mesh [22]. However, when applying this method to injection moulding simulation and solving the initial value problem with e.g. a Runge-Kutta method, this requires storage of the complete velocity field for every time step. Thus, tremendous storage capacity is required. To get around this problem, in [11] a method is proposed using conservation of identity for MCIM by defining material particles by their unique identity (e.g. material, colour, place and time of injection). The transport of the identity during the flow can be described by a pure convection equation

$$\dot{\underset{\sim}{\xi}} = \frac{D\underset{\sim}{\xi}}{Dt} = \underset{\sim}{0} \quad \text{in } \Omega_m, \quad \text{with} \quad \underset{\sim}{\xi}(\vec{x},t) = \underset{\sim}{f}(\vec{x},t) \text{ on } \Gamma_e, \qquad (2)$$

where $\dot{\underset{\sim}{\xi}}$ is the material derivative and $\underset{\sim}{\xi}$ is for instance a column containing those properties of the particles that are considered important, like the starting position and time (x_0,y_0,z_0,t_0), the viscosity, colour, etc. Γ_e is the injection area and Ω_m the cavity geometry (Fig. 2). The problem of particle tracking is solved here with an Eulerian approach (fixed frame of reference). Then the conservation of identity can be expressed as

$$\frac{\partial\underset{\sim}{\xi}}{\partial t} + \vec{v}\cdot\vec{\nabla}\underset{\sim}{\xi} = \underset{\sim}{0}, \qquad (3)$$

where $\partial\underset{\sim}{\xi}/\partial t$ is the spatial derivative. In this representation the change of label values in space is calculated instead of tracking pre-defined particles. The actual tracking can be carried out by determining the positions of a given set of labels in time if materials with identical material properties are used. For use in MCIM, label values at the end of filling provide all the necessary information: i.e. where and when all particles at present position, did enter the mould. By defining a specific, desired shape and position of a second component inside a product, only the label values of these particles have to be determined to know what configuration should have been injected to realize this desired multi-component product. The main advantage of this method is the use of field information rather than tracking a set of particles. For further details, see below in Section 2.4, inverse mapping.

2.2 Bifurcation of the Midsurface

In the case of bifurcation of the midsurfaces, like e.g. in the presence of stiffener ribs positioned perpendicular to the

flow direction, the flow has to be splitted to fill both the rib and the remaining part. All existing $2\frac{1}{2}$-D codes have problems in this respect, since the pressure is calculated by satisfying the local conservation of mass at the flow splittings in a weak sense by forcing that the sum of the inflow volume fluxes equals the sum of the outflow fluxes. However, in calculating the history dependent properties such as the convected temperature, density, visco-elastic stresses, orientation, conversion and the identity or colour of particles, copying of the gapwise distribution of properties from an upstream branch to the downstream branches is not allowed since local conservation of identity is not satisfied. To overcome the problem of cloning the material particles, the bifurcations should be treated differently. When modelling the flow splittings correctly [25, 26], it is shown that, for example the resulting gapwise temperature profiles in the downstream branches are changed considerably when compared to the results of the existing simulation codes. An initial symmetric profile in an upstream branch results in asymmetric temperature profiles in the downstream branches, which in turn induces warpage of the product. The solution to this problem as used in present work, is described under Section 3.3.

2.3 Front Flow

In mould filling, two flow regimes can be distinguished: the main flow domain and a front flow. In the last, the fountain effect occurs while in the main flow a simple 2D stratified flow situation exists (Fig. 2). The so-called fountain flow [27] occurs in flows with one or more free boundaries and a no-slip condition at the walls causing fluid elements adjacent to the moving front to spread towards the walls (Fig. 3(a)) since fluid elements near the center move at a higher speed than the local average speed across the channel. The fountain flow affects the particle distribution in moulded products, especially for material elements close to the mould walls. Also, break-through of core layers towards the surface of a product is completely controlled by the fountain region. For those reasons it is important to incorporate the fountain flow in the modelling of moulding processes.

In the idealized fountain flow, the residence time is neglected and a simple model, based on conservation of mass, is applied [13, 18, 28]. In this approach, the fountain flow region simplifies to a single straight line that moves with the average front velocity $\bar{v}_s$ (Fig. 3(b)).

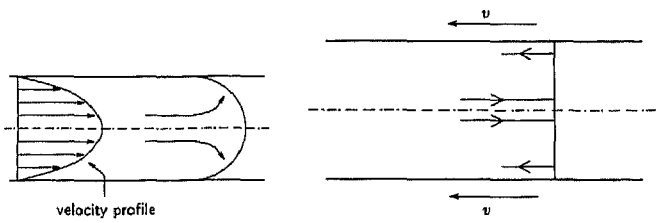

(a) Fountain flow phenomena (b) simplified front model

Fig. 3. Fountain effect in injection moulding

For some applications, the residence time in the fountain flow region is of importance, e.g. in the case of multi-component or in reactive injection moulding [29]. For a Newtonian fluid, the semi-analytical model of Bhattacharji and Savic [30] gives the opportunity to derive a relation between the residence time in the front flow and the inflow or outflow position [11]. The original model gives an analytical expression of the velocity field in the fountain region from which the flow paths can be constructed. The residence time as function of the inflow or outflow position can be computed by integrating along a flow-path until the particle re-enters the main flow. This representation can be parameterized by fitting the curves obtained with a polynomial function. In doing so, not much extra computing effort is required for incorporating the residence time distribution into a front model.

For non-Newtonian viscosity models, the gapwise velocity profile does not correspond to the parabolic profile of a Newtonian fluid. Therefore, the model of Bhattacharji et al. can only be applied when information with limited precision is needed.

2.4 Inverse Mapping

The ultimate goal of simulation of the injection moulding process, is to predict the process conditions given the required product properties. In the case of MICM it is important that one can predict the injection sequence beforehand, since for complex geometries it is almost impossible to do this by trial-and-error. The task to be completed can be summarized as:

> Given the particle distribution at the end of the filling stage and the definition of a required layer distribution, determine the injection configuration and sequence necessary in order to attain that pre-set definition.

For one-component flow, such as occurring in multi-colour injection, the label field contains all the information necessary to determine the injection configuration and the inverse mapping can be carried out straightforward (as a post-processing task). For multi-component flows, however, the material distribution influences the flow kinematics. In that case the injection configuration has to be obtained iteratively:

1. Perform a filling simulation with one component.
2. Determine the injection sequence given the required material distribution.
3. Perform a multi-component filling simulation with the injection sequence determined under steps 2 as input.
4. Repeat steps 2 and 3 until the injected and calculated injection sequences correspond to a sufficient degree.

It is important to note that there is no guarantee that this iterative process will converge. However it is our experience that for low Reynolds number flows, as is the case in MCIM, convergence is established.

3 Numerical Aspects

3.1 Temporal Discretization

The time derivatives that occur in the equations are all material derivatives. The material derivative of an arbitrary

variable α is formally defined by

$$\frac{D\alpha}{Dt} \overset{\text{def}}{=} \dot{\alpha} \equiv \lim_{\theta \to 0} \frac{\alpha(\vec{x},t+\theta\,\Delta t) - \alpha(\vec{s},t)}{\theta\,\Delta t}, \tag{4}$$

where $\vec{s}$ denotes the position at time t of the particle that is located at $\vec{x}$ at time $t+\Delta t$. Eq. (4) cab be approximated as:

$$\dot{\alpha}_{n+1} \approx \frac{\alpha_{n+1} - \alpha_c}{\Delta t_{n+1}}, \tag{5}$$

where $\alpha_{n+1} = \alpha(\vec{x},t+\theta\,\Delta t)$ and $\alpha_c = \alpha(\vec{s},t)$. Now, it remains to determine the convected variable α_c. Consider $\alpha_c \overset{\text{def}}{=} \alpha(\vec{s}(\vec{x},t_{n+1}),t_n)$ as a field variable. This field can be obtained by convecting the variable field at $t=t_n$, $\alpha_n \overset{\text{def}}{=} \alpha(\vec{x},t_n)$ by the known velocity field $\vec{v}(\vec{x},t)$. Hence, the variable α_c is determined by solving

$$\frac{\partial \alpha_c}{\partial t} + \vec{v} \cdot \vec{\nabla}\alpha_c = 0, \quad \alpha_c(t_n) = \alpha_n. \tag{6}$$

Using this method, the convection operator can be splitted from the remainder of the equation. Although it differs from the operator splitting technique, where the convection operator is part of a larger operator as appears in e.g. the convection-diffusion equation or differential models in visco-elastic flow calculations (see e.g. [31, 32]), the procedure is the same. The procedure can be summarized as follows: The solution field at $t-\Delta t$ is convected by a known velocity field. The outcome of this calculation provides the initial condition for the remaining part of the original equation for the current time step. The advantage of this method is that different numerical schemes can be used for solving different terms in the equations. Especially in the case of convection dominated problems this is a great benefit, since the classical schemes often show spurious oscillations.

3.2 Spatial Discretization

The spatial discretization is performed by using a finite element method, with meshes as shown in Fig. 4. The pressure problem requires a mesh that covers the midplane of the product (Fig. 4(a)). The discretization is performed using biquadratic quadrilateral elements defined in $\mathbb{R}^2$ with one degree of freedom – the pressure – per node [33]. Since realistic injection moulding products are three dimensionally shaped, the elements are situated in a 3D space.

The temperature problem is solved using one-dimensional finite element meshes consisting of linear elements in the gapwise direction of the product (Fig. 4(b)). These 1D-meshes are present in every vertex node (nodal point) of the 2D mesh of the pressure problem, which are named the gridlines. The nodal points of the 1D-meshes are called the gridpoints.

Finally, the convection problem – for determining the convected variables and particle tracking – is solved on meshes of bilinear quadrilateral elements in $\mathbb{R}^2$ [33]. These meshes are formed by the gridplanes (Fig. 4(b)) which are the 2D planes spanned by the gridpoints.

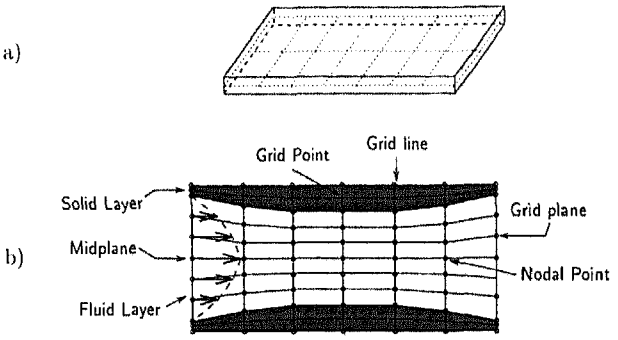

Fig. 4. Spatial discretization in midplane (a) and perpendicular to that (b)

3.3 Solution of the Particle Tracking Problem

The convection equation is solved on a finite element mesh consisting of bilinear quadrilateral elements coinciding with the gridplanes that are situated in the fluid layer (Fig. 4(b)). The gridplanes are slightly curved in the direction of the flow following the shape of the already solidified layer. In this way a rough approximation of the (small) velocity component v_3^s is established (without explicitly calculating it), since the gridpoints are equally divided between the midplane and the solid/liquid interface.

The time derivative in Eq. (3) is approximated by a two-step θ-method [34], where θ is a parameter in the interval $0 < \theta \leq 1$. For $\theta = 1$ the scheme reduces to the Euler implicit method which has an accuracy of $\mathcal{O}(\Delta t)$, while the Crank-Nicholson scheme appears for $\theta = 0.5$ which is $\mathcal{O}(\Delta t^2)$ accurate. Because of its relatively high accuracy this last scheme is chosen in the calculations. The solution of Eq. (3) is carried out with the Streamline Upwind Petrov Galerkin (SUPG) finite element method [35]. The SUPG method provides stable solutions in case of convection dominated flows with discontinuities in the solution as may occur in the particle tracking problem. However, still some numerical dispersion may occur both down- and upstream of such a discontinuity.

As explained in Section 2.2, in the case of bifurcations of the midsurface, unrealistic distributions in the downstream parts are found when using the $2\frac{1}{2}$D approach for the particle identity [25]. The (improved) strategy in resolving the convection problem is to split the product geometry into parts that contain no bifurcations, but that can be considered as 2D flow geometries. At the intersections, the values at the inflow boundaries of the downstream branches are prescribed as inflow boundary conditions (Dirichlet condition). Then, the convection problem is solved for each part separately, irrespective of the order of filling. After convection, the values at the inflow boundaries of the downstream branches are updated using the calculated values at the outflow branches of the upstream sections. Hereby, it is assumed that the time steps taken are small enough so that the material particles do not cross the opposite element boundaries, which is in fact the well known Courant-Friedrichs-Lewy (CFL) condition [36].

During updating the values at the downstream inflow boundaries, local mass conservation has to be satisfied. Suppose that there are n outflow boundaries and m inflow boundaries. For every inflow boundary i the fractional thickness $f_{i,j}$ of connected outflow boundaries j that fills the inflow part is determined by a local mass balance. Let $f_{i,j} = [f^-, f^+]$, then the fractional thickness can be determined by solving

$$\int_{f^-}^{f^+} v_j^*(z)\, dz = q_i, \tag{7}$$

where $v_j^*(z)$ is the velocity profile of the outflow boundary j and q_i the volume flux at the inflow boundary i. An additional relation has to be formulated to determine the positions f^-, f^+ completely. For that purpose, the spatial sequence of the element groups around a connection node is taken into account. For example in the case of two inflow nodes connected with one outflow node $f_{1,1} = [-h/2, f^+]$ and $f_{2,1} = [f^+, h/2]$. Whether a connection curve is an inflow or outflow boundary is checked by evaluating the dot product $(\vec{V}^* p \cdot \vec{n})$ with $\vec{n}$ the outward normal vector parallel to the midplane.

The gapwise values of any property to be convected can be distributed over the connected downstream points by mapping the values in the fractional thicknesses of the upstream points to the inflow gridlines. In this way, local conservation of mass is only weakly satisfied. A further improvement is to preserve mass conservation by evaluating

$$\int_{z_1}^{z_k} v_d^*(\zeta)\, d\zeta = \int_{f_{i,j}}^{s} v_u^*(\zeta)\, d\zeta \quad k = 2, \ldots, nf, \tag{8}$$

where v_d^*, v_u^* are the gapwise velocities at the down- or upstream nodes, respectively, and s the gapwise position at which the value has to be determined. This latter method can also be applied when an abrupt change of thickness exists at the interconnection between two parts. This could be useful when the shape of the velocity profile is expected to change much with in- or decreasing flow rate, e.g. when using shear-thinning liquids or materials with a yield stress.

4 Multi-Component Injection Moulding: Some Examples

Since modelling of injection moulding and particle tracking are combined in one simulation code (VIp [26, 37]), filling with multi-colours or even multi-components can be studied. In this section, several characteristics will be elucidated with the aid of three different examples: (i) co-injection of a strip, (ii) filling a product with a bifurcation, and (iii) inverse mapping in order to determine the injection sequence for a desired colour or even material distribution.

4.1 Co-Injected Strip with Ribs

Experimental results were obtained in a cooperation between Philips Centre for Manufacturing Technology, Eindhoven, The Netherlands and the Du Pont European Technical Centre where the products were moulded. The different test series are described in [11] and [38].

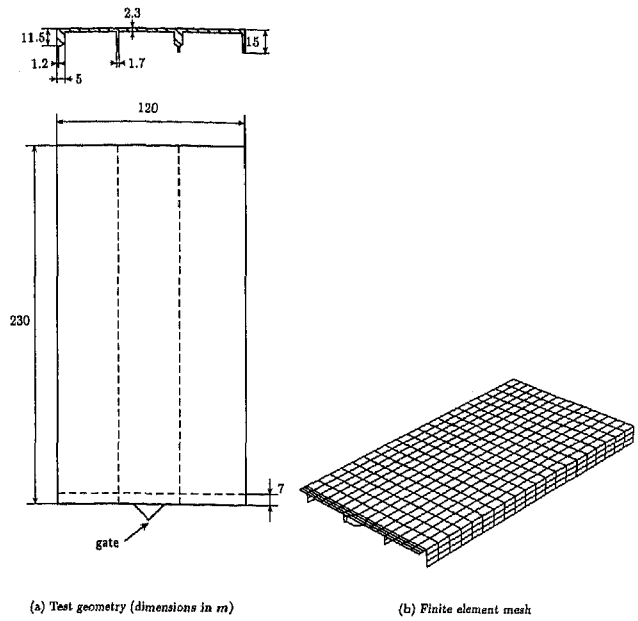

Fig. 5. Coinjected strip with ribs

4.1.1 Experimental Conditions

The product consist of a strip of 230 × 120 × 2.3 mm with 4 stiffener-ribs and a beam-like edge (see Fig. 5(a)). The ribs are 12.7 mm in height and have different cross-sections. The beam-like edge (7 × 9 × 120 mm), acting as a flow divider, connects the strip with the runner section. The product is filled by sequential injection of two differently coloured nylons (PA66). The material data are taken from Peters et al. [11], who used a Truncated Power Law model for the viscosity:

$$\eta(T,\dot{\gamma}) = \begin{cases} m_0\, e^{-\beta T/n} \phi^{1-n} & \text{for } \dot{\gamma} \le \dfrac{1}{\phi} e^{\beta T/n}, \\ m_0\, e^{-\beta T} \dot{\gamma}^{n-1} & \text{for } \dot{\gamma} > \dfrac{1}{\phi} e^{\beta T/n}. \end{cases} \tag{9}$$

with $n = 0.61$, $m_0 = 3.455 \cdot 10^4$ Pas, $\phi = 0.347$ s, and $\beta = 0.0175\ K^{-1}$. The density and thermal properties are listed in Table 1.

The colour first injected was white-translucent, followed by the second which was blue. They are also referred to as skin and core material respectively. The strips were injected in a mould with a constant temperature of 348 K using

Table 1. Specification density and thermal properties

	PA66	
	Melt	Solid
ϱ kg m^{-3}	950	1 140
λ W/(m K)	0.1346	0.27
c_p J/(kg K)	2 897	2 432

Table 2. Processing conditions test series PA1–PA6

Series	T_{inj} [K]		swp
	Skin (1)	Core (2)	
PA1	571	556	67 %
PA2	571	556	50 %
PA3	571	556	22 %
PA4	571	556	56 %
PA5	574	573	56 %
PA6	556	568	56 %

different processing conditions. In particular the injection temperature of the two materials and their relative fractions were altered, see Table 2. The core material is injected after the product has been filled up to the volume percentage given by the switch point swp. The measured filling time proved to be about 1.9 s for product including runners (with a total volume of $1.16 \cdot 10^{-4}$ m^3), thus the actual flow rate was about $6.1 \cdot 10^{-5}$ m^3/s. In the calculations the runner section is not taken into account, leaving the volume

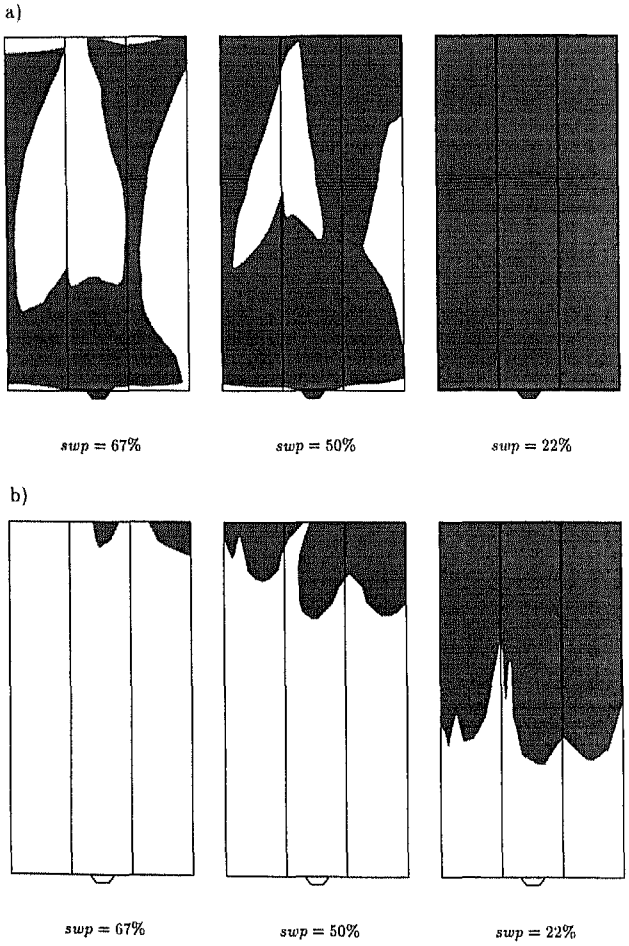

Fig. 6. Experimental material distribution in the midplane (a) and break-through areas (b). Influence of switch point ($T_{inj1,2}$ = 571 556 K)

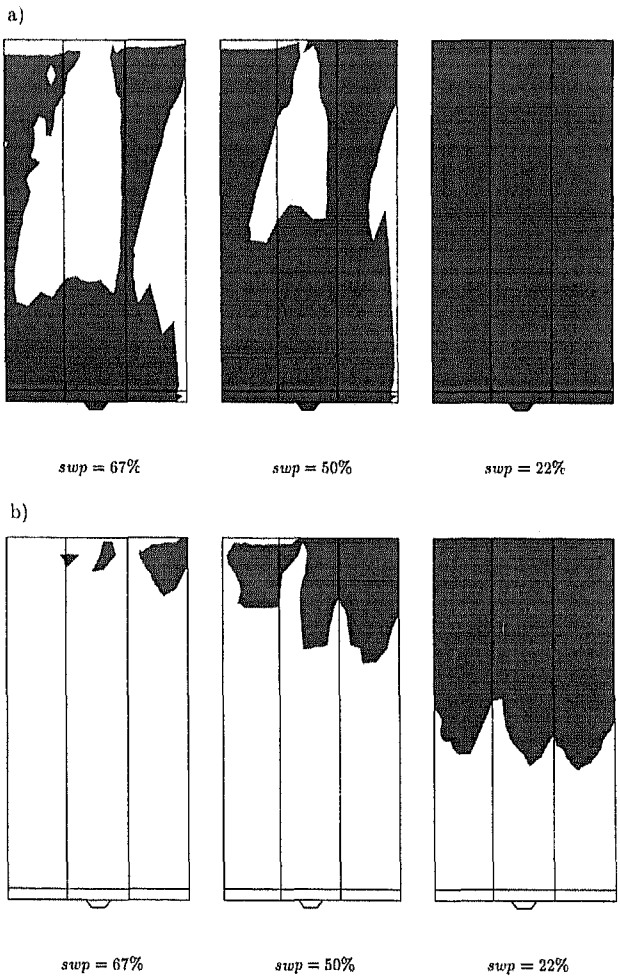

Fig. 7. Calculated material distribution in the midplane (a) and break-through areas (b). Influence of switch point ($T_{inj1,2}$ = 571 556 K)

to be filled $1.00 \cdot 10^{-4}$ m^3. The finite element mesh covering the midplane of the cavity is plotted in Fig. 5(b). Since no details about the exact temperature (distribution) are known, cooling is assumed to be symmetrical over the thickness direction and a Biot-type of boundary condition is chosen with a heat transfer coefficient of H = 3 000 W/(m^{2}K). This value has proven to give a cyclic variation of the mould wall temperature that is in the range of values measured in some test moulds in our lab. The main points of interest in this example are:

- application to relatively complex geometries should be possible, since this is the aim of the simulations.
- the simulation code should be able to predict the influence of the main processing conditions on the material/colour distribution in the product.
- a proper prediction of break-through of the first injected material by the second injection material is required, because the occurrence of undesired break-through is one of the most common problems to solve in practice of multi-component moulding.

4.1.2 Validation of the Numerical Simulations

The colour distribution is used for visual validation of the results. Since the skin material is translucent, the skin/core material distribution can be determined easily without cutting the sample in pieces. The same holds (but to a somewhat less extent) for the areas where the blue core material breaks through the skin material and ends up at the product surface. Since with sequential injection the material, or its colour, only changes in time, the calculated injection time labels provide the necessary information for visualization of the final distribution. In this case, a colour contour plot provides sufficient information. The two contour levels that coincide with the switch time and the total filling time are needed, respectively. The core material distribution is, subsequently, visualized by constructing these contour plots in the midplane of the product, while the break-through areas are easily found by plotting the label field at the surface.

The influence of the switch point on the material distribution is shown in the Figs. 6 and 7 for the experimentally and the numerically obtained results, respectively. Figs. 6(a) and 7(a) clearly show that the thick ribs act as flow leaders

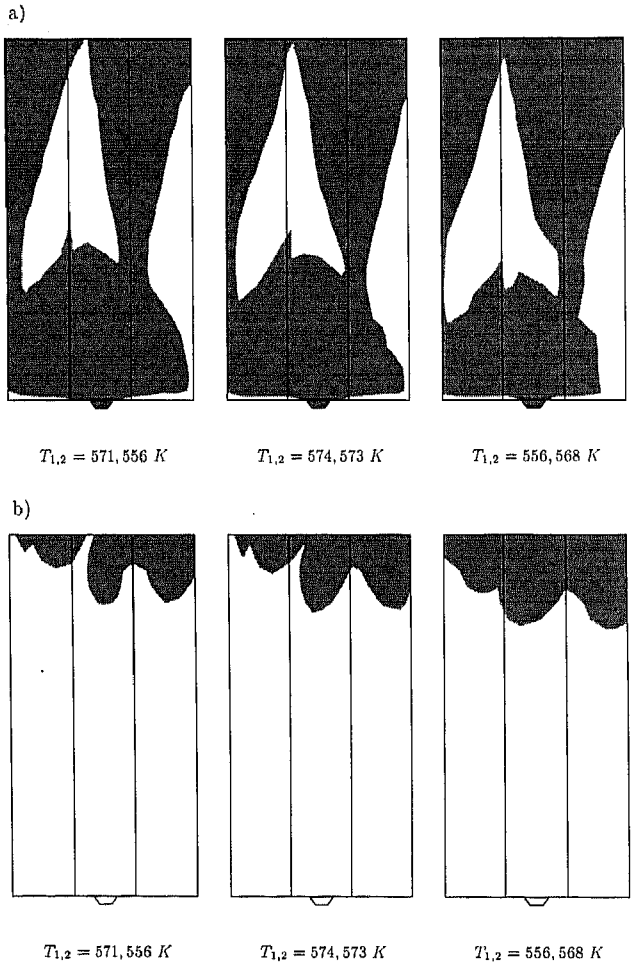

Fig. 8. Experimental material distribution in the midplane (a) and break-through areas (b). Influence of melt temperature (swp = 56 %)

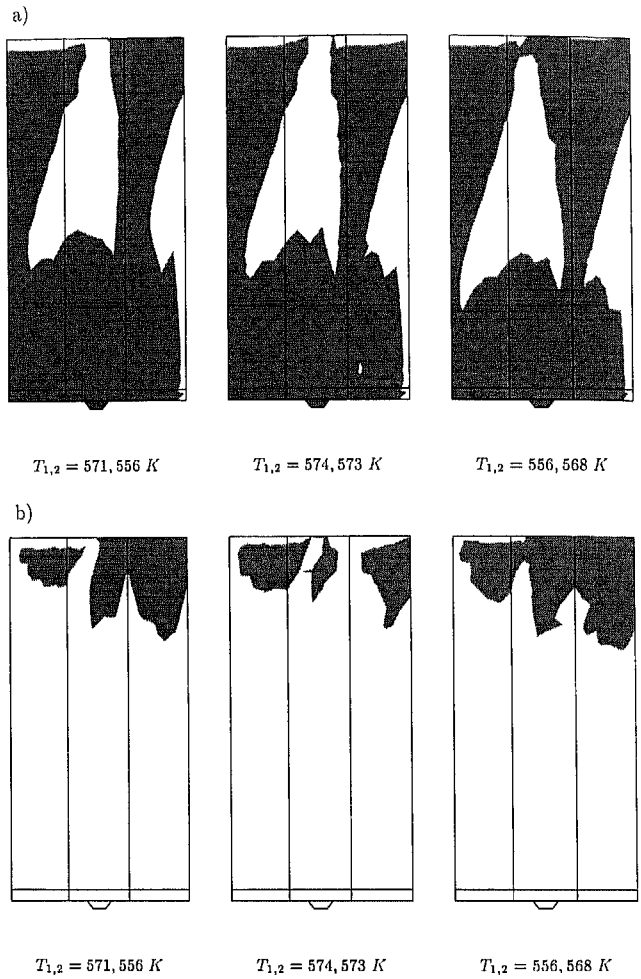

Fig. 9. Calculated material distribution in the midplane (a) and break-through areas (b). Influence of melt temperature (swp = 56 %)

and make the second material penetrating into (or in between) the first material. If the switch-point number is decreased, more blue material is injected. This is clearly demonstrated in the midplane but also the break-through area grows (see Figs. 6(b) and 7(b)). Comparing the predicted colour distributions with the experimental ones for the different processing conditions, a strikingly good resemblance is found. Only the presence of some skin material in the flow divider is not found, because no solidified layer is formed at the edges of a product when employing the $2\frac{1}{2}$-D approach. Also the amount of first material that remains in the midplane is slightly underpredicted at the righthand side of the product.

The effect of the initial skin and core temperature is demonstrated in Figs. 8 and 9. Although the variation in temperature is only small, a noticeable influence on the distribution is found in both experiments and numerical predictions. The mechanism that is responsible for this effect, is the growth of the solidified layers during the injection. The lower the melt temperature of the first, white material, the thicker the solidified layer will be. Then, more second, blue, material will flow through the thicker ribs

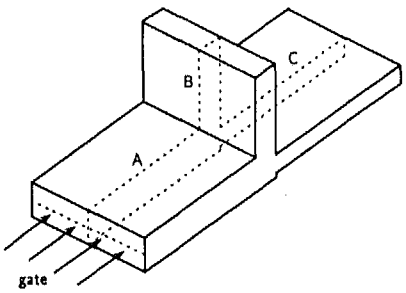

Fig. 10. Schematic drawing of the T-shaped strip

which have the lowest flow resistance. As a consequence, the area occupied by the white material in the midplane is shifted towards the gate and the break-through area is somewhat larger. Even for these extreme small changes in processing conditions a remarkably good agreement between the numerical simulations and the experiments is obtained. Note that for some cases the numerically determined break-through areas are disconnected from the upper end while this is not the case for the corresponding experimental results (Figs. 6 to 9). Also in the midplane, the blue material does not reach the upper end while theoretically this should be the case if there is any break-through in that area. This defect can be explained by numerical errors that are induced at the end of the filling stage. Since the thick ribs act as flow leaders, at the end of filling, the region between those ribs will be partly filled transversely instead of longitudinally by these flow leaders. This sudden change in the direction of the velocity, mainly in the upper left end of the part, and the corresponding extreme changes in direction of convection, are not captured well enough by the numerical scheme used.

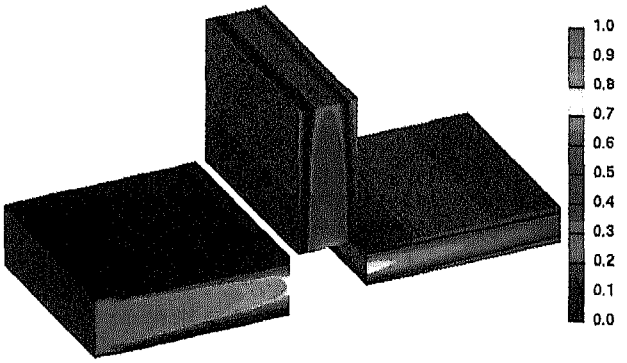

(a) Injection time label

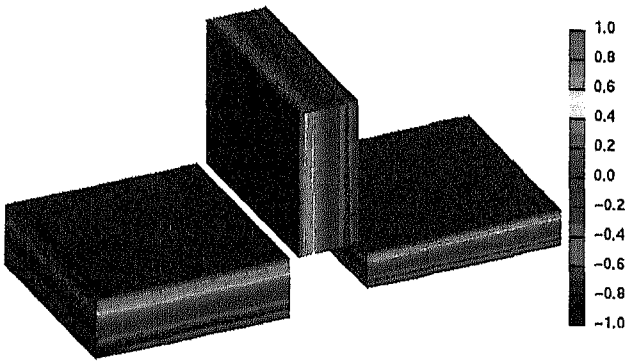

(b) Injection position label

Fig. 11. (Incorrect) gapwise label distribution in cross-section T-strip, according to existing computer codes

4.2 Bifurcation of the Midsurface

The most elementary geometry of a bifurcation is found in a T-shaped strip (Fig. 10). The strip as used here consist of three branches (A,B,C) with the dimensions (length × width × thickness): A: 40 × 40 × 2.5 mm, B: 30 × 40 × 2.5 mm, and C: 40 × 40 × 1.5 mm. The flow can be considered as so-called one-dimensional, since the strip is fed by a line-gate over the full width of the sample and results are considered only in the mid-cross-section of the sample, represented by the dashed line in Fig. 10. In the $2\frac{1}{2}$D approach, the midplanes of all distinct branches that form the total product are interconnected. Consequently, a small overlap exists in the connections. For clearness, the three branches of the T-shaped strip of Fig. 10 are disconnected.

The material properties are those typical for a polystyrene. The parameters for the Cross model are: $\eta_0 = 4.76 \cdot 10^{10}\, e^{(-25.74(T-373))/(61.06+T-373)}$, $n = 0.252$, and $\tau^* = 3.08 \cdot$ Pa. The main processing conditions are:

- flow rate $Q = 9.4 \cdot 10^{-6}$ m^3/s (injection time $t_{inj} = 1.0$ s),
- melt temperature $T_{inj} = 503$ K,
- mould temperature $T_{wall} = 323$ K.

Asymmetry of the gapwise temperature profiles is allowed for. The boundary condition chosen for the temperature is again the Biot condition with $H = 3\,000$ W/(m^{2}K). The results of the calculations performed using the strategy of existing computer codes can be found in Fig. 11(a) for the injection time label distribution (t-label) and Fig. 11(b) for the gapwise injection position (z-label). The label values are made dimensionless with the injection t_{inj} and the half gap width $h/2 = 1.25$ mm respectively. The injection time labels visualize the distribution of the residence time, which equals $1 - t_{label}$, over the product and, moreover, coincide with the material distribution in sequential moulding. The colour contours in the two downstream branches differ, since the dimensions are chosen such that branch B is filled completely before C. The gapwise entrance position z, however, is hardly influenced by this filling behaviour. Fig. 11(a) and 11(b) clearly demonstrate the effect of the fountain flow on the label distributions: the colour originally injected in the midplane can be found at the surface. The z-label distribution shows clearly that the gapwise distribution of label values in both downstream branches are similar which is in conflict with the conservation of identity principle. The results when using the local mass balance to divide the material particles over the two downstream branches are

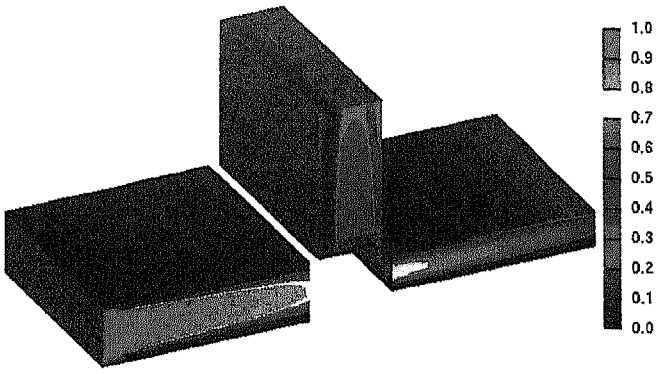

(a) Injection time label

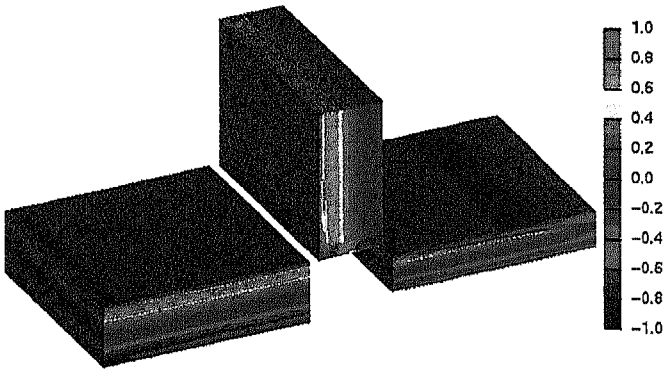

(b) Injection position label

Fig. 12. Correct gapwise label distribution in cross-section T-strip, according to present code

given in Figs. 12(a) and 12(b). These are the (approximated) correct results which differ essentially with those of Fig. 11(a) and 11(b). The z-label distribution in branch B only contains values originated from the upper half of the feeding branch A whereas branch C contains both label values that stem from the lower part as well as from the upper part. The latter particles have entered branch C after branch B has been filled completely. The most important difference between both approaches can be found at the surface of branch C where particles that are injected in the lower half of the gap-width end up at the upper surface of this branch when preserving conservation of identity. From these results, it can be concluded that for practical applications, where break-through often is undesirable, the correct approach should be employed.

Finally, the effect of the proper splitting technique for history dependent properties is demonstrated in Figs. 13(a) and 13(b). In these figures the gapwise temperature profiles at different positions along the flowpath are plotted. Again, a considerable influence of the local mass conservation on the overall distribution can be observed.

4.3 Inverse Mapping

In this section, two examples are given of the inverted problem which can be formulated as: determine the configuration that has to be injected to attain the requested material distribution in the product. In the first example, a product with increased complexity is moulded using multi-colour moulding whereas the application of an iterative technique is demonstrated for the filling of a simple rectangular mould with dissimilar materials.

4.3.1 Multi-Colour Moulding

The product considered is drawn schematically in Fig. 14(a) by the finite element mesh of the midplane (each element has a dimension of 10×10 mm). It consists of a square plate ($80 \times 80 \times 2.5$ mm) with an opening (30×30 mm) and a rib ($30 \times 30 \times 1.5$ mm). The plate is filled in 1.0 s through a line gate of 20 mm in width. The material used is a polystyrene (PS). The processing conditions are the same as used in the previous example.

The melt front advancement is plotted in Fig. 14(b). The rib is initially filled up to about 30 %, then the melt in the rib stops flowing and, only after the remaining of the plate has been filled completely, the melt front in the rib starts to move again. Due to this filling behaviour, and the presence

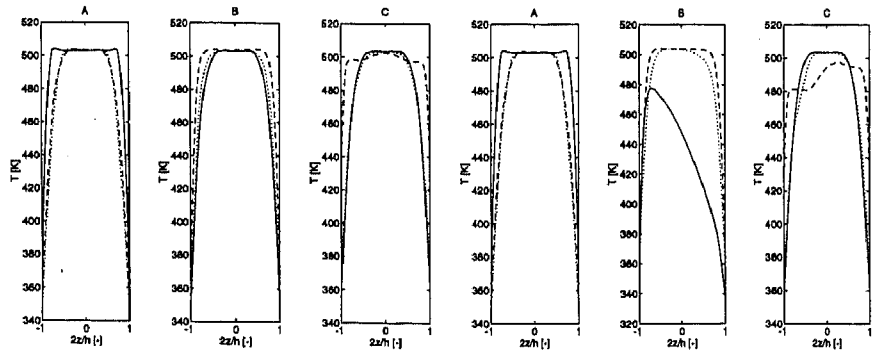

(a) Incorrect approach

(b) Correct approach

Fig. 13. Gapwise temperature profiles at different positions along the flowpath of each separate branch (begin: full line, halfway: dotted line, end: dashed line)

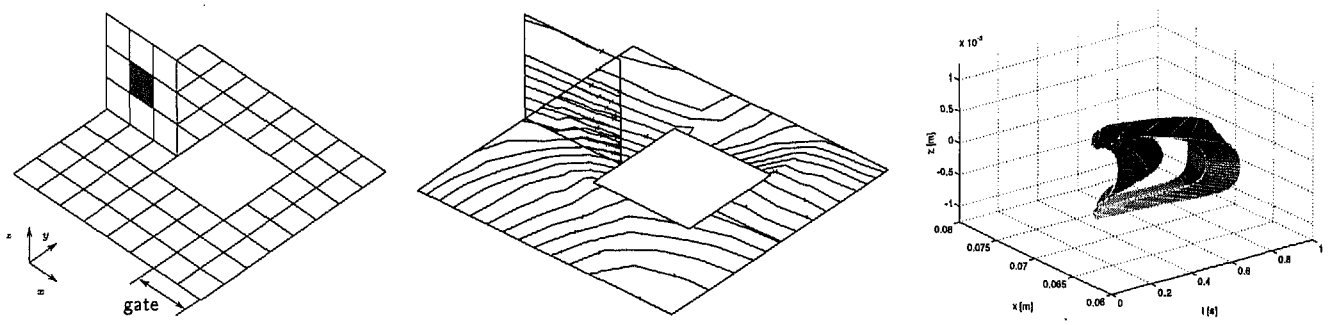

(a) Finite element mesh

(b) Calculated flow front positions (the increment of the adjacent contour lines is 0.05 *s*)

(c) Injection configuration obtained by the inverse mapping

Fig. 14. Example of inverse mapping for multi-colour injection moulding

of the flow splitting, the label distribution in the rib in the small part behind it are complicated. The task to accomplish, as an example, is to make the shaded area in the rib (see Fig. 14(a)) to be of a different colour over the entire gap-width. The inverse mapping can be performed easily by looking for the label values, i.e. the injection time label and the entrance position coordinate labels. The information can be translated into a two-coloured pre-form, which can be injected into the mould by a plunger system, by multiplying the injection time with an average filling speed. The distribution of the coloured material in such a pre-form is represented by the 3D-shape plotted in Fig. 14(c). Thus, to reach our goal, a box-like volume (of dimensions: $20 \times 2.5 \times \bar{v}t$ mm) containing the volume rendered in Fig. 14(c) of a differently coloured material has to be established.

In order to derive the machine settings from the data obtained by the inverse mapping, another visualization method can be employed. One possible method is to slice the volume at constant injection times to establish cross-sections of the injection configuration. These data are easier to interpret than the 3-D structure depicted here. One should realize that the calculated injection configuration can not be made in a simple manner. A flexible distribution device or a two-step production process using a pre-form [10] are needed to approximate these configurations. However, the method gives the contours of the domain that should not be crossed in order to prevent, for example, break-through or too thin internal layers.

4.3.2 Multi-Material Moulding

A rectangular strip of dimensions $200 \times 50 \times 3$ mm is chosen for demonstration of the iterative technique in the inverse mapping procedure. The task to accomplish is to establish a layer of a lower-viscosity material in the upper half of the product (Fig. 15(b)). Starting with a simulation with only one component, the injection configuration is determined and, subsequently, again injected in a multi-component simulation. This procedure is repeated until the shape of the required distribution has been converged to a sufficient degree. The processing conditions and the material (PS) are similar to those used in the previous examples except for the material that should occupy the layer (refered to as material X) which differs only in viscosity. The viscosity of this (artificial) material equals $\eta = \eta_{PS}/3$.

Fig. 15(a) shows the injection configuration after the first iteration step when no viscosity difference is taken into

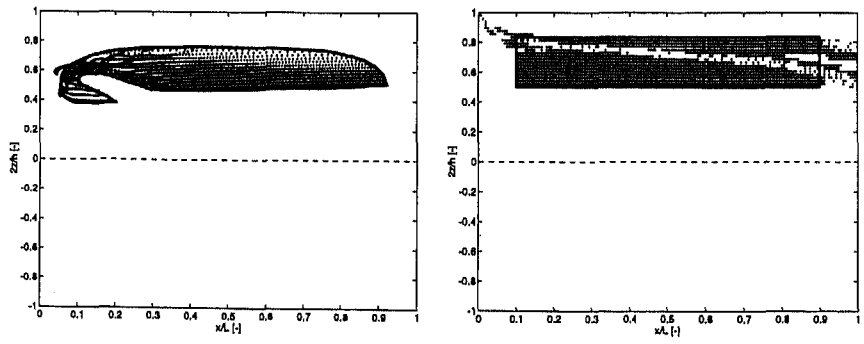

(a) Injection configuration

(b) Required material distribution and result after injecting the estimated configuration

Fig. 15. Initial condition inverse mapping procedure

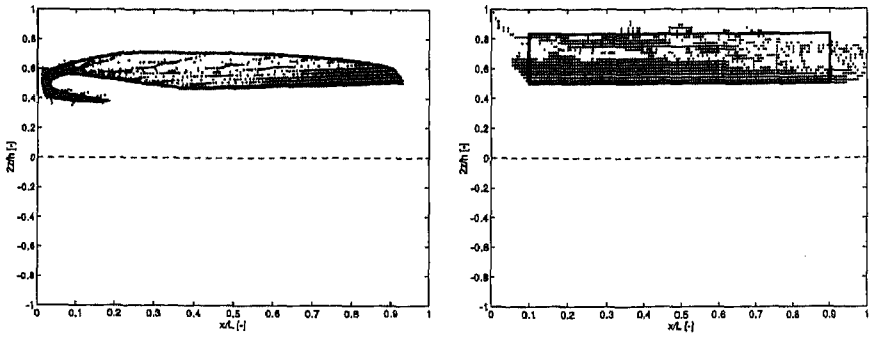

(a) Injection configuration

(b) Required material distribution and result after injecting the estimated configuration

Fig. 16. Converged results inverse mapping procedure (third iteration)

account. The shape is obtained by plotting points that formed initially a dense grid in the rectangle. Note that these points do not represent material elements since they have no volume. This configuration gives, after one component injection, the points in Fig. 15(b). From this figure it is clear that many points are above the so-called folding line (the white area that crosses the layer) and thus experienced the fountain effect. This causes steep gradients in the numerical label solution field which are difficult to handle by the numerical convection scheme. Due to the numerical inaccuracies of the convection scheme (numerical dispersion and diffusion which causes non-unique labels) and the imperfect flow front model, some points are outside the region that is considered to be occupied by material X. Nevertheless, this configuration of 15(a) is taken as the reference condition for further iterations. The procedure given above is repeated, but now with the injection configuration consisting of the two materials, until conversion was reached (no visible change of the injection configuration). Three iterations proved to be sufficient. The final configuration obtained in this way is plotted in Fig. 16(a) and the corresponding material distribution after injection is shown in Fig. 16(b). Comparing the initial with the final injection configuration, the influence of the viscosity difference of the two materials is clearly visible.

Concluding, it can be stated that for this multi-component problem the inverse mapping technique can be applied iteratively to determine the injection configuration required. Application of the procedure to more complex shaped products and larger differences in material behaviour need further investigation. In spite of some irregularities in the injection configurations, caused by numerical deficiencies in calculating the label identities, especially for the material elements that have experienced the fountain flow, the method proved to be promising.

5 Conclusions

The simulation of the filling stage in multi-component injection moulding (MCIM) can be accomplished by adding an extra conservation law – the conservation of identity of material particles – to the existing set of equations that generally defines the $2\frac{1}{2}$D approach. In that approach the conservation of mass is only weakly satisfied. Improving this formulation by enforcing a local mass conservation at the front line and at flow splittings, the distribution of material particles in an injection moulded product can be predicted more accurately. As a consequence, a meaningful prediction of the material distribution in MCIM, or those final properties of an injection moulded product which are affected by the history dependent variables like temperature, density, visco-elastic flow-induced stresses and the degree of reaction, is only possible if the improved method is employed.

The mathematical formulation of the particle tracking problem results in hyperbolic (scalar) convection equations which can be solved adequately by the Streamline Upwind Petrov Galerkin (SUPG) finite element method. The same method can be applied to solve the material derivatives when the convective operator is splitted from the remainder of the equations.

In MCIM the break-through of the second injected material through the first injected material is completely governed by the fountain effect at the flow front. Even for geometrically simple products, the material (or colour) distribution turned out to be rather complex. Therefore, assistance of computer simulations is indispensable to achieve the desired material distribution in the product. The effect of preserving the local mass balance at flow splittings, results in asymmetric gapwise profiles of history dependent properties or identity labels in the downstream branches whereas they were symmetrical in the upstream part.

In order to define the injection sequence and/or configuration that should result in the requested material distribution, an inverse calculation has to be performed. Using the conservation of identity method, this calculation reduces to an inverse mapping. The inverse mapping can be carried out straightforward, provided that the determined injection configuration does not change the flow kinematics. This is e.g. the case in simple multi-colour injection. In the case of real multi-material injection, however, an iterative technique has to be adopted in which the multi-colour mapping is taken as the initial configuration. To obtain detailed information in the inverse mapping procedure, the spatial discretization of the geometrical model of the product has to be relatively fine due to the large deformations that are induced by the fountain effect.

6 Recommendations

Some limitations of the existing techniques/modelling has been met. Therefore some recommendations for future research can be given

- for injection moulded products where the ratio of thickness to flowlength is large (h/L > 1), more detailed information at flow splittings or at the front region could be obtained by using local 'perpendicular' 2D calculations in those regions. Instead of connecting the midplanes, then the small 2-D regions take care of those connections in the case of flow splittings. The analogous 2D fountain region can be thought to be attached to the flow front.
- For relatively small products with a ratio of thickness to flowlength close to unity, a complete 3-D analysis is more appropriate. The melt flow front advancement could be modelled by a polymer/air interface represented by a high (polymer) and low (air) viscosity material applying the fixed domain approach [39].
- The effect of the correct approach at the flow splittings and abrupt changes of thicknesses should be incorporated in the calculations of the final properties of a product, since history dependent properties like temperature, density, visco-elastic stresses, orientation and conversion, require that the conservation of identity is satisfied.

References

1 *Garner, P. J., Oxley, D. F.:* British patent 1, 156, p. 217 (1969)
2 *Eckardt, H.:* J. of Cellular Plastics 23, p. 555 (1987)
3 *Eckardt, H.:* Kunststoffe 75, p. 145 (1985)
4 *Tung, T. T., Kudert, F. G.:* SPE ANTEC Tech. Papers 36, p. 760 (1990)
5 *Donovan, R. C., Rabe, K. S., Mammel, W. K., Lord, H. A.:* Polym. Eng. Sci. 15, p. 774 (1975)
6 *White, J. L., Lee, B. L.:* Polym. Eng. Sci. 15, p. 481 (1975)
7 *Young, S. S., White, J. L., Clark, E. S., Oyanagi, Y.:* Polym. Eng. Sci. 20, p. 798 (1980)
8 *Turng, L. S., Wang, V. W., Wang, K. K.:* J. of Eng. Mat. Techn. 115, p. 48 (1993)
9 *Schlatter, G., Davidoff, A., Agassant, J. F.:* SPE ANTEC Tech. Papers 41, p. 456 (1995)
10 *Vos, E., Meijer, H. E. H., Peters, G. W. M.:* Int. Polym. Process. 6, p. 42 (1991)
11 *Peters, G. W. M., van der Velden, P. J. L., Meijer, H. E. H., Schoone, P.:* Int. Polym. Process. 9, p. 258 (1994)
12 *Hieber, C. A., Shen, S. F.:* J. Non-Newtonian. Fluid Mech. 7, p. 1 (1980)
13 *Sitters, C. W. M.:* Numerical Simulation of Injection Moulding. PhD thesis, Eindhoven University of Technology (1988)
14 *Boshouwers, A. H. M., van der Werf, J. J.:* Inject-3, A Simulation Code for the Filling Stage of the Injection Moulding Process of Thermoplastics. PhD thesis, Eindhoven University of Technology (1988)
15 *Douven, L. F. A.:* Towards the Computation of Properties of Injection Moulded Products: Flow- and Thermally Induced Stresses in Amorphous Thermoplastics. PhD thesis, Eindhoven University of Technology (1991)
16 *Tucker, C. L., III:* Fundamentals of Computer Modeling for Polymer Processing. Hanser, Munich 1991
17 *Isayev, A. I.,* (Ed): Injection and Compression Molding Fundamentals. Marcel Dekker, Inc., New York, 1987
18 *Dupret, F., Vanderschuren, L.:* AIChE. J. 34, p. 1959 (1988)
19 *Chiang, H. H., Hieber, C. A., Wang, K. K.:* Polym. Eng. Sci. 31, p. 116 (1991)
20 *Baaijens, F. P. T.:* Rheol. Acta 30, p. 284 (1991)
21 *Zoller, P.:* J. Polym. Sci. 20, p. 1453 (1982)
22 *Crochet, M. J., Davies, A. R., Walters, K.:* Numerical Simulation of Non-Newtonian Flow. Elsevier, Amsterdam 1984
23 *Luo, X.-L., Tanner, R. I.:* J. Non-Newt. Fluid Mech. 22, p. 61 (1986)
24 *Luo, X.-L., Mitsoulis, E.:* Int. J. Num. Meth. Fluids 11, p. 1015 (1990)
25 *Couniot, A., Dheur, L., Dupret, F.,* in: Proc. of the IMA Conference on Mathematical Modelling for Materials Processing 1991. *Cross, M., Pittman, J. F. T., Wood, R. D.* (Eds.), p. 381. Oxford University Press 1993
26 *Zoetelief, W. F.:* Multi-Component Injection Moulding. PhD thesis, Eindhoven University of Technology (1995)
27 *Rose, W.:* Nature 191, p. 242 (1961)
28 *Manas-Zloczower, I., Blake, J. W., Macosko, C. W.:* Polym. Eng. Sci. 27, p. 1229 (1987)
29 *Castro, J. M., Macosko, C. W.:* AIChE. J. 28, p. 250 (1982)
30 *Bhattacharji, S., Savic, P.,* in: Proc. 1965 Heat Transf. Fluid Mech. Inst. *Charwat, A. F.* (Ed.), p. 248. Stanford University Press (1965)
31 *Donea, J.:* App. Mech. Rev. 44, p. 205 (1991)
32 *Baaijens, F. P. T.* Applied Computational Mechanics 2, lecture notes. Eindhoven University of Technology, The Netherlands 1992
33 *Segal, A.:* SEPRAN, user manual, standard problems and programming guide. Ingenieursbureau SEPRA, Leidschendam, The Netherlands 1984
34 *van de Vosse, F. N.:* Numerical Analysis of Carotid Artery Flow. PhD thesis, Eindhoven University of Technology (1987)
35 *Brooks, A. N., Hughes, T. J. R.:* Comp. Meth. Appl. Mech. Eng. 32, p. 199 (1982)
36 *Hirsch, C.:* Numerical Computation of Internal and External Flows, 1, 2. John Wiley & Sons, Chicester 1990
37 *Caspers, L. W.:* VIp, An Integral Approach to the Simulation of Injection Moulding. Prediction of Product Properties. PhD thesis, Eindhoven University of Technology (1995)
38 *Hendriks, R. D. H. M.:* Technical Report CTB541-92-5035, Philips Centre for Manufacturing Technology, Eindhoven 1992
39 *Haagh, G. A. A. V, Zuidema, H., van de Vosse, F. N., Peters, G. W. M., Meijer, H. E. H.:* Int. Polym. Process. 12 (1997)

Date received: August 1996
Date accepted: December 1996

Acknowledgements

Financial support from the Commission of the European Communities is gratefully acknowledged (Contract BREU-495 Brite Euram, Project BE-4076). Furthermore, we acknowledge Philips Centre of Manufacturing Technology, Eindhoven for kindly providing us with the results of the co-injected strip.